ECOLOGY

Cell size, density, and nutrient dependency of unicellular algal gravitational sinking velocities

Teemu P. Miettinen[1]*†, Annika L. Gomez[2]†, Yanqi Wu[1]†, Weida Wu[1,3], Thomas R. Usherwood[1,4], Yejin Hwang[1], Benjamin R. K. Roller[5], Martin F. Polz[5]*, Scott R. Manalis[1,3,6]*

Eukaryotic phytoplankton, also known as algae, form the basis of marine food webs and drive marine carbon sequestration. Algae must regulate their motility and gravitational sinking to balance access to light at the surface and nutrients in deeper layers. However, the regulation of gravitational sinking remains largely unknown, especially in motile species. Here, we quantify gravitational sinking velocities according to Stokes' law in diverse clades of unicellular marine microalgae to reveal the cell size, density, and nutrient dependency of sinking velocities. We identify a motile algal species, *Tetraselmis* sp., that sinks faster when starved due to a photosynthesis-driven accumulation of carbohydrates and a loss of intracellular water, both of which increase cell density. Moreover, the regulation of cell sinking velocities is connected to proliferation and can respond to multiple nutrients. Overall, our work elucidates how cell size and density respond to environmental conditions to drive the vertical migration of motile algae.

INTRODUCTION

Algae are a genetically, morphologically, and biophysically diverse group of photosynthetic microorganisms. Algae comprise the base of the marine food webs and are responsible for approximately 75 to 90% of marine carbon fixation by mass (*1*). Consequently, the sinking of algal material—either in the form of single cells or as components of larger sinking particles, such as marine snow (*2*–*4*)—is a key contributor to the "biological pump," which sequesters carbon dioxide from the atmosphere to deep oceans and marine sediments (*5*). Hence, a quantitative understanding of sinking velocities of different algae is needed for modeling marine ecosystems and carbon fluxes, especially in the context of global change (*2*, *6*–*12*).

The vertical position of live cells affects their growth, viability, and community composition, as both organic and inorganic nutrients are more abundant deeper in the ocean while light is stronger at the surface (*7*, *12*, *13*). Hence, algae are under ecological pressure to adjust their position in the water column according to their need for nutrients and light. To adjust their vertical position, algae can alter their gravitational sinking and motility, but live cell sinking and sedimentation rate measurements cannot decouple gravitational sinking from motility. Consequently, studies on gravitational sinking have focused on nonmotile species, which can adjust their gravitational sinking by regulating cell size and composition (*14*–*18*). The extent to which gravitational sinking is regulated in motile species remains unclear, and the molecular mechanism(s) responsible for such sinking regulation are unknown even in most nonmotile species.

[1]Koch Institute for Integrative Cancer Research, Massachusetts Institute of Technology, Cambridge, MA 02139, USA. [2]Department of Civil and Environmental Engineering, Massachusetts Institute of Technology, Cambridge, MA 02139, USA. [3]Department of Biological Engineering, Massachusetts Institute of Technology, Cambridge, MA 02139, USA. [4]Harvard-MIT Department of Health Sciences and Technology, Institute for Medical Engineering and Science, Massachusetts Institute of Technology, Cambridge, MA 02139, USA. [5]Division of Microbial Ecology, Centre for Microbiology and Environmental Systems Science, University of Vienna, Vienna, 1030, Austria. [6]Department of Mechanical Engineering, Massachusetts Institute of Technology, Cambridge, MA 02139, USA.
*Corresponding author. Email: teemu@mit.edu (T.P.M.); martin.f.polz@univie.ac.at (M.F.P.); srm@mit.edu (S.R.M.)
†These authors contributed equally to this work.

Gravitational sinking velocity depends on the cell's size, density, and drag force from seawater. For spherical cells, this can be derived from the Stokes' law (*3*, *6*, *14*, *15*)

$$V_s = \frac{2(\rho_{cell} - \rho_{fluid})gr^2}{9\mu} \quad (1)$$

where ρ_{cell} is the density of the cell, ρ_{fluid} is the density of the surrounding fluid, g is the gravitational acceleration, r is radius of the cell, and μ is the dynamic viscosity of the fluid. A cell dimension–dependent correction factor can be applied to Eq. 1 for nonspherical particles (*15*, *19*). This approach has been widely used to estimate sinking velocities based on microscopy observations of cell radius, but cell density is rarely known or measured, especially for single cells. Consequently, little is known about the cell size and cell density dependency of sinking velocities on a single-cell level.

We reasoned that independent measurements of cell volume and buoyant mass could be used to calculate sinking velocity without assumptions about cell density (Fig. 1A). Buoyant mass, m_b, is defined as

$$m_b = V(\rho_{cell} - \rho_{fluid}) \quad (2)$$

where V is the volume of the cell. As the fluidic density is typically known, cell density and, consequently, sinking velocity can be found from buoyant mass and volume. Here, we obtain direct measurements of single-cell volumes and buoyant masses to define algae sinking velocities across different species, cell sizes, densities and nutrient conditions. Our work reveals examples of motile species that increase their sinking velocity upon starvation, and we uncover the mechanistic basis behind this sinking velocity regulation. Overall, our results allow us to propose a qualitative ecological model where the regulation of cell size and composition affects the marine carbon pump and nutrient cycles.

RESULTS

Characterizing sinking velocities across phylogenetically diverse algal species and single cells

We sought to establish an approach for measuring gravitational sinking velocities across algal species and across single cells within a

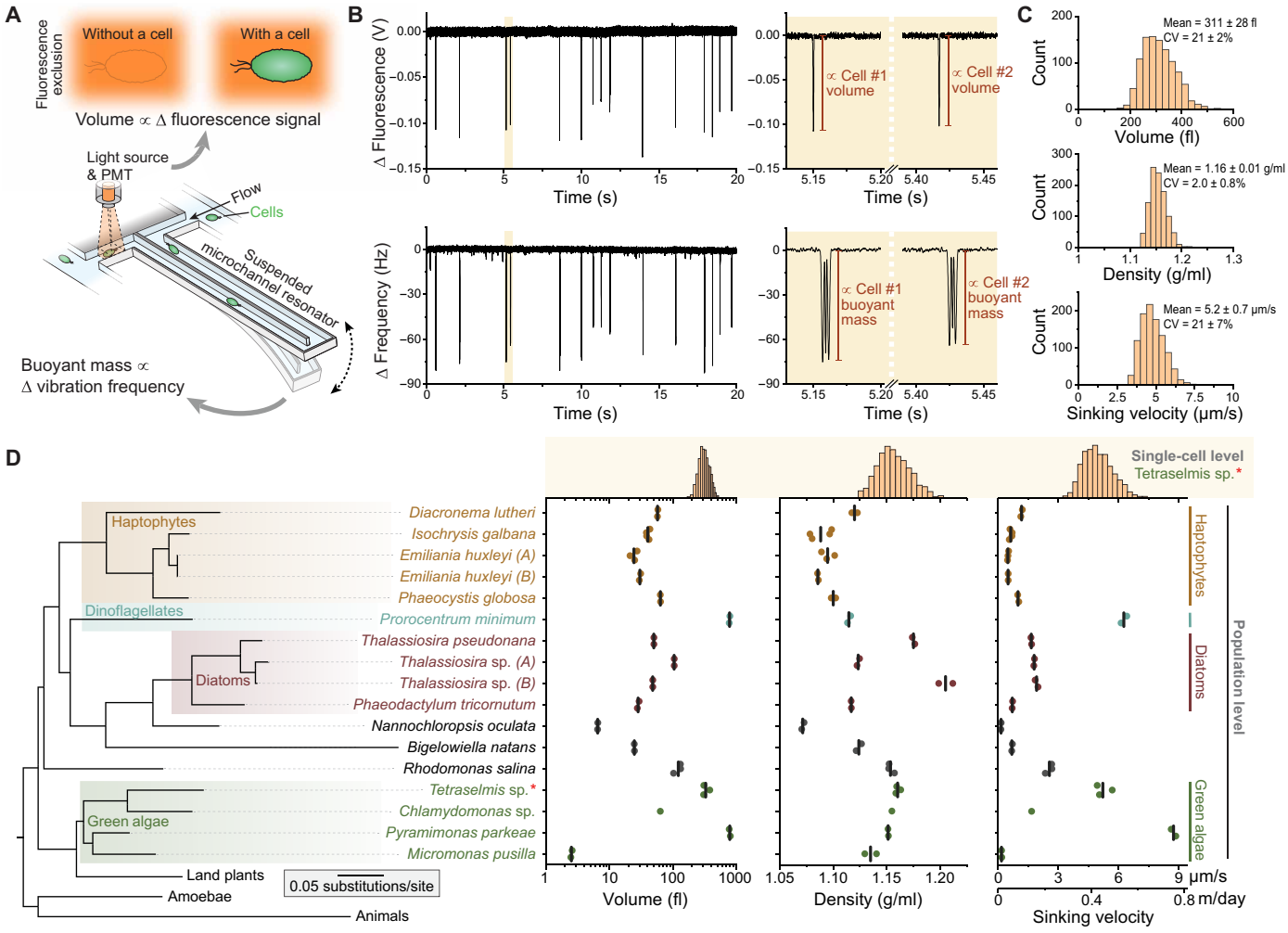

Fig. 1. Gravitational sinking velocities across phylogenetically diverse algae species and single cells. (**A**) Schematic of the measurement approach. To determine gravitational sinking velocities according to Stokes' law on a single-cell level, we coupled the SMR-based buoyant mass measurements with fluorescence exclusion–based volume measurements. PMT, photomultiplier tube. (**B**) Left: Representative raw data for fluorescence exclusion measurements (top) and buoyant mass measurements (bottom) for the species *Tetraselmis* sp. Right: Zoom-ins displaying data for two example cells. (**C**) Representative single-cell volume, density, and sinking velocity histograms for *Tetraselmis* sp. (n = 1027 single cells). The listed statistics depict mean ± SD from five independent cultures. (**D**) Left: A phylogenetic tree of the measured algae species according to 18*S* rRNA. Animals, amoebae, and land plants are shown for reference. The major clades of algae are color coded. Right: Cell volumes, densities, and sinking velocities for each species. Dots depict independent cultures, and vertical lines depict mean values. Top: Representative histograms of single-cell volumes, densities, and sinking velocities for the species *Tetraselmis* sp.

species. We coupled the suspended microchannel resonator (SMR) (*20*–*23*) with fluorescence exclusion–based volume measurements (*24*) (Fig. 1A) to determine the volume and density of each cell (*25*). The SMR is a microfluidic mass sensor, where cells flow through a microchannel that is embedded in a vibrating cantilever. This changes the vibration frequency of the cantilever proportionally to the buoyant mass of the cell (Fig. 1B). Next to the SMR cantilever, our system incorporates a fluorescence detection area, where the fluorescence signal decreases proportionally to the volume of a cell travelling through, as the cell excludes cell-impermeable fluorophore-containing media from the detection area (Fig. 1B). For a ~12-μm-diameter particle, our typical SMR buoyant mass precision is ~0.1% (*26*), and our volume precision by fluorescence exclusion is ~1% (*25*), although both precisions are size dependent (*21*, *25*). Thus, we can precisely determine single-cell volume and buoyant mass, which we use to calculate cell density and sinking velocity for individual algal cells (Eqs. 1 and 2).

To the best of our knowledge, single-cell densities and gravitational sinking velocities have never been reported for motile algae. We characterized two unicellular eukaryotic algal species: *Tetraselmis* sp., which is an industrially relevant green alga with high lipid production capacity and uses in aquaculture (*27*, *28*), and *Prorocentrum minimum*, which is a globally distributed, bloom-forming dinoflagellate that produces toxins affecting shellfish populations and human health (*29*). The single-cell densities of *Tetraselmis* sp. displayed a coefficient of variation (*CV*) of 2.0 ± 0.8% (mean ± SD) (Fig. 1C), which is an order of magnitude more than what is observed in typical eukaryotic model systems (*30*). Consequently, there was substantial cell-to-cell variability in sinking velocities with *CV* values of 21 ± 7% (mean ± SD). *P. minimum* displayed even

higher variability in single-cell densities (*CV* of 2.7 ± 0.7%, mean ± SD) and sinking velocities (*CV* of 38 ± 9%, mean ± SD) than *Tetraselmis* sp. (fig. S1A). Thus, cell densities and sinking velocities in algae are more variable than expected based on observations in other model systems.

In addition to our single-cell approach for determining sinking velocity, we used a population level approach to examine a range of unicellular algal species. Using the SMR and Coulter counter to measure buoyant masses and cell volumes, respectively, we characterized cell densities and sinking velocities in 17 unicellular eukaryotic algal species spanning all major clades of algae, including haptophytes, dinoflagellates, diatoms, and green algae (Fig. 1D, left, and fig. S1B). All species were verified using 18*S* ribosomal RNA (rRNA) sequencing and grown under autotrophic conditions in high nutrient media. The measured species spanned ~2.5 orders of magnitude in volume from the ~2.5 fl of green alga *Micromonas pusilla* to the ~785 fl of green alga *Pyramimonas parkeae* (Fig. 1D and datasets S1 and S2). Despite the wide phylogenetic and cell volume range of the studied species, cell densities ranged only ~12% between the species. We also observed significant density variation between two separate isolates of the diatom *Thalassiosira* sp. (Fig. 1D), thus demonstrating the degree of density variation possible among closely related taxa. Cell sinking velocities ranged ~410% between species, from 0.2 μm/s in *Nannochloropsis oculata* to 12.8 μm/s in *P. parkeae*. We also examined the cell shape dependency of sinking velocities by correcting the calculated sinking velocities according to previously established shape-dependent correction factors (*19*). This revealed that the shape dependency was minimal (dataset S3), and all sinking velocities reported in figures therefore assume a spherical cell shape. Overall, these results reveal the interspecies heterogeneity in cell densities and sinking velocities and indicate that our measurement approach is suitable for a wide size and phylogenetic range of algal species.

In oceans, individual algae species are often dispersed across wide vertical distances. Similarly, the sinking of individual cells may not be well represented by the mean sinking velocity of the population. To provide context for our single-cell observations of cell density and sinking velocity, we compared the cell-to-cell variation observed in *Tetraselmis* sp. to the species-to-species variation. The density variation within a species (*CV* ~2%) is similar in magnitude to the density variation between species (*CV* ~3%) (Fig. 1D). Single-cell sinking velocities also varied across a wide part of the sinking velocity range observed across species (Fig. 1D, top). These results suggest that, in addition to active motility and cell aggregation, the variability of cell sinking velocities could result in algal dispersal across wide vertical ranges in oceans. We did not observe any systematic differences in cell densities or sinking velocities between motile and nonmotile species ($P = 0.79$ and $P = 0.09$, respectively, Welch *t* test).

⅔-Power law scaling of sinking velocities with cell volume

Understanding the cell volume dependency of cell sinking is critical for ecological modeling, especially as cell sizes are predicted to decrease with warming oceans (*31*, *32*). Stokes' law predicts that cell sinking velocities scale with cell volumes according to the ⅔-power law (Eq. 1), assuming cell volume–independent densities. However, cell densities have not been systematically defined for most algae, making it unclear whether density is uniform across different volumes. Previous studies have suggested that algae sinking velocities scale with cell volume with a scaling factor that is significantly less than ⅔, implying that density may decrease with increasing cell volume or that cell shapes may be highly volume dependent (*33*, *34*). We used our dataset (Fig. 1D) to examine the volume dependency of cell densities and sinking velocities across species using regression models with and without phylogenetic information. In both models, cell volumes did not correlate with cell densities (Fig. 2A), but cell volumes displayed a strong correlation with sinking velocities (Fig. 2B). More than 90% of the sinking velocity variation was accounted for by cell volumes ($R^2 = 0.92$ to 0.95), whereas only ~30% of the sinking velocity variation could be accounted for by cell densities ($R^2 = 0.31$; fig. S2A). The sinking velocities scaled with cell volumes with a scaling exponent of ~0.73 ± 0.04 (mean ± SE). The size scaling of cell sinking was similar when analyzing all tested species or only the motile species, whereas nonmotile species displayed a higher scaling exponent (fig. S2B). Overall, both regression models displayed comparable results, indicating that cell volume, density, and sinking velocity have little phylogenetic signal.

Our single-cell measurements also enabled us to examine the volume dependency of cell densities and sinking velocities within a species. In *Tetraselmis* sp. and *P. minimum*, cell densities were not correlated with cell volumes (Fig. 2, C and E), but both cell volumes and cell densities displayed a modest correlation with sinking velocities (R^2 ~ 0.4 to 0.5; Fig. 2, D and F, and fig. S2, C and D). Single-cell sinking velocities scaled with cell volumes with a scaling exponent of 0.6 to 0.7 (Fig. 2, D and F). Similar results were obtained when cells were grown under low nutrient conditions (datasets S4 and S5).

Overall, these results show that cell densities are not cell volume dependent, resulting in approximately ⅔-power law scaling of sinking velocities both within and between species. Consequently, when comparing vastly different sized species (e.g., an order of magnitude difference in cell volumes), cell volume can be used as a proxy for sinking velocities. However, when comparing algal cells with similar volumes, such as cells from the same population, cell density differences have a more prominent impact on the sinking velocities, as indicated by the R^2 values when correlating cell density (or volume) with sinking velocity. In these situations, cell density differences need to be considered. Next, we explore situations where cell sinking velocities change due to cell density changes.

Nutrient limitation increases sinking velocity by increasing cell density in a species-specific manner

Cell volumes are known to depend on environmental nutrient conditions with higher nutrient conditions typically supporting higher cell volumes (*35*). However, little is known about how cell densities, or sinking velocities, change with environmental nutrient conditions. We therefore examined the nutrient dependency of sinking velocities. We compared four algae species following 5-day culture under high and low nutrient conditions. The species investigated were *Bigelowiella natans* (chlorarachniophyte), *Phaeodactylum tricornutum* (diatom), *Tetraselmis* sp., and *P. minimum*. The species differed in their nutrient responses, with most pronounced responses observed in *Tetraselmis* sp. (Fig. 3A) and *P. minimum,* both of which increased their masses under low nutrient conditions while maintaining nearly constant cell volumes (Fig. 3B). Consequently, *Tetraselmis* sp. and *P. minimum* displayed significantly increased cell densities and sinking velocities under low nutrient conditions (Fig. 3, C and D). We did not observe any systematic morphological

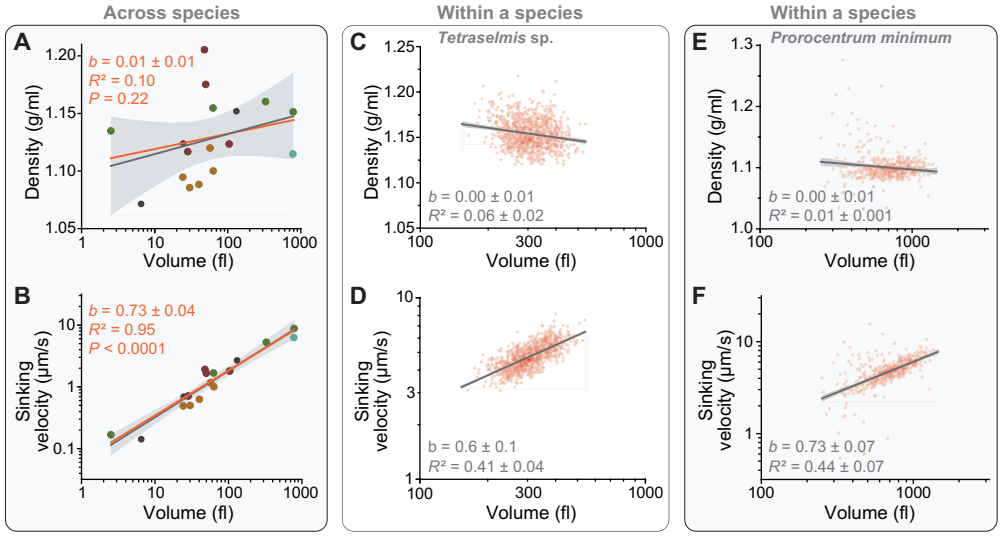

Fig. 2. Sinking velocities display ⅔-power law scaling with cell volumes across and within species. (**A** and **B**) Correlation between cell volumes and cell densities (A) or sinking velocities (B) across all species shown in Fig. 1D. Dots depict mean values for each species ($N = 17$), which are color-coded according to their major clade. Data were fitted with linear regression models with (orange) and without (gray) phylogenetic information, and shaded areas indicate 95% confidence bands for the latter model. (**C** and **D**) Representative experiment displaying the correlation between cell volumes and cell densities (C) or sinking velocities (D) for individual *Tetraselmis* sp. cells (red dots, $n = 1027$ cells). Gray lines and shaded areas indicate linear regressions and 95% confidence bands, respectively. The listed statistics were calculated from five separate experiments. (**E** and **F**) Same as (C) and (D), but data are for species *P. minimum* ($n = 484$ cells).

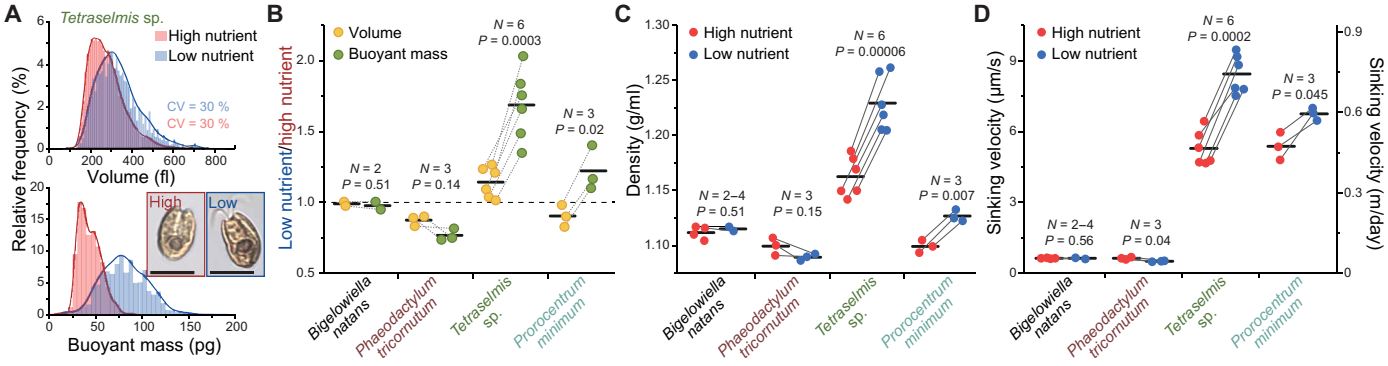

Fig. 3. Starvation increases sinking velocity by increasing cell density in a species-specific manner. (**A**) Single-cell mass and volume histograms for *Tetraselmis* sp. in high (red) and low (blue) nutrients. Inset displays representative images of the cells. Scale bars, 5 µm. (**B**) Change in cell volume (yellow) and buoyant mass (green) between low and high nutrient conditions in indicated species. (**C** and **D**) Cell density (C) and sinking velocity (D) under high (red) and low (blue) nutrient conditions in indicated species. All samples were grown under high light conditions. In (B) to (D), *N* indicates the number of independent cultures as depicted by dots, paired samples are connected by a line, and horizontal lines depict mean values. *P* values were obtained by pair-sample *t* test.

differences between the two nutrient conditions in *Tetraselmis* sp. (Fig. 3A), despite the low nutrient conditions resulting in a stationary phase (starvation) (fig. S3A). Thus, our results highlight the need for direct cell mass (or density) measurements when studying cell sinking regulation. More broadly, these results show that cells can adjust their sinking velocities significantly upon changes in environmental nutrient conditions, likely reflecting an adaptation that allows starving algae to sink faster to deeper, nutrient richer waters. However, the sinking velocity responses to nutrient limitation were species specific, as *B. natans* did not display any nutrient responses despite starvation under the low nutrient conditions (Fig. 3, B to D, and fig. S3A), and *P. tricornutum* decreased its sinking under low nutrient conditions (Fig. 3, B to D). This species specificity may arise from differences in macromolecular composition between species or from different temporal dynamics of the starvation response (see Supplementary Note for details).

Carbohydrate accumulation and loss of intracellular water enables sinking velocity increases

We aimed to understand the mechanistic basis for nutrient-dependent sinking velocity regulation in more detail using *Tetraselmis* sp. as a model system. Because the increased cell densities and sinking velocities under starvation were caused by the addition of cell mass, we sought to determine whether photosynthesis is required for this mass increase. We examined cell density and sinking velocity under varying nutrient and light conditions following a 5-day culture. This

revealed that the complete absence of light prevented the cells from increasing their density and sinking velocity under the low nutrient conditions (Fig. 4, A and B). Measurements of cell proliferation revealed that the cells entered starvation after 2 days of low nutrient conditions but not under high nutrient conditions when light was present (fig. S3B). However, proliferation was stopped in the absence of light independently of nutrient availability across the time course (fig. S3B), as expected for a photoautotrophic species under autotrophic conditions (Fig. 4, A and B). Thus, stopping cell proliferation does not automatically increase sinking velocities. More broadly, the mechanism by which cells accumulate mass to increase their density and sinking velocity requires photosynthesis.

Next, we studied how *Tetraselmis* sp. alter their composition to achieve the higher cell mass under low nutrient conditions. We characterized the protein, lipid, and carbohydrate content of the cells in relation to the cells' dry mass. This revealed that under low nutrient conditions, the cells contain less proteins, but significantly more carbohydrates, than under high nutrient conditions (Fig. 4C). Overall, these results indicate that the starvation-induced cell mass increases in *Tetraselmis* sp. can be explained by photosynthesis-driven accumulation of carbohydrates.

While carbohydrate accumulation can increase cell mass, cell density is also dependent on other cellular components, including cellular water content. We used known densities of macromolecules and the typical macromolecular composition of *Tetraselmis* sp. to simulate how cell densities change upon carbohydrate accumulation (see Supplementary Note for details). This revealed that while carbohydrate accumulation will increase cell density, it alone is insufficient to explain the cell density difference between high and low nutrient conditions (fig. S4A). Instead, our calculations suggested that cells must also lose intracellular water. To test this hypothesis, we characterized dry volume of *Tetraselmis* sp. cells using a previously established approach where cells' buoyant mass is measured in normal and heavy water to derive dry volume (*23*, *36*). By comparing these dry volume measurements to Coulter counter–based total volume measurements, we observed that *Tetraselmis* sp. cells contain more dry volume but less water when starved (Fig. 4D). The cells displayed a fractional water content of ~50% (v/v) under high nutrient conditions but only ~25% under low nutrient conditions (Fig. 4E). As indicated by our simulations (fig. S4, B and C), this loss of intracellular water will increase cell density significantly. Thus, the cell density and sinking velocity increases we observe between high nutrient condition and starvation condition can be explained by the accumulation of carbohydrates and the loss of intracellular water. Notably, regulation of intracellular water has been identified as a buoyancy regulating mechanisms in other algae species (*16*), and other model systems are also known to adjust their water content upon starvation (*25*, *37*).

Cell sinking velocities respond to multiple nutrients and are coupled with cell proliferation

Surface ocean nutrient levels vary spatially and temporally. While nitrogen is the most common growth-limiting nutrient, other nutrients can also become growth limiting (*13*). To understand the

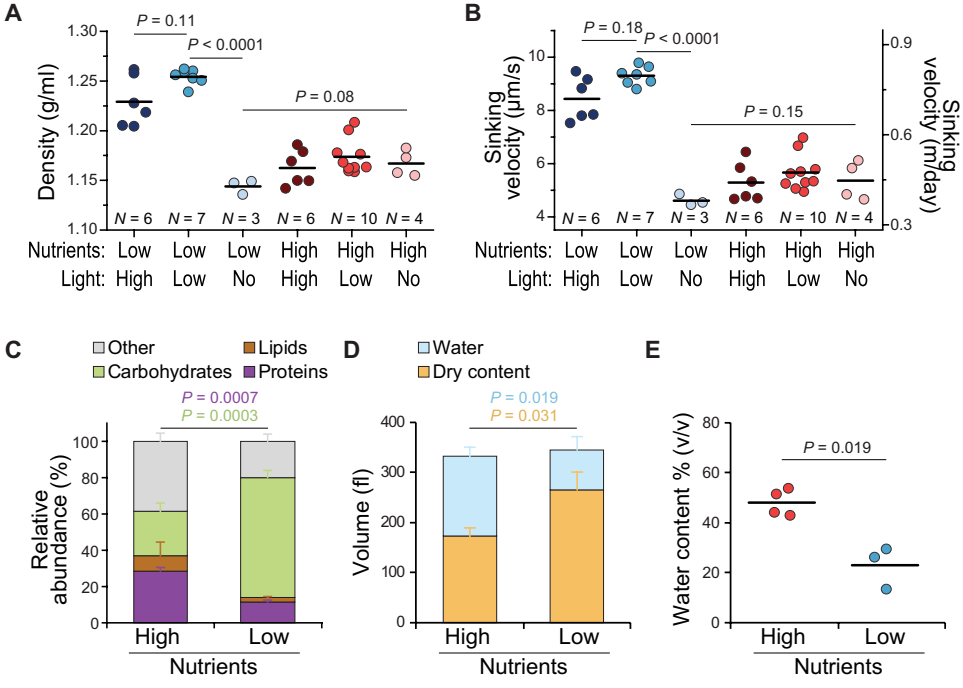

Fig. 4. Starved *Tetraselmis* sp. increases sinking velocity by photosynthesis-driven accumulation of carbohydrates and by a loss of intracellular water. (**A** and **B**) *Tetraselmis* sp. cell densities (A) and sinking velocities (B) under indicated nutrient and light conditions after 5-day culture. *P* values were obtained by analysis of variance (ANOVA) and Tukey's post hoc test. Dots depict independent cultures, horizontal lines depict mean values, and *N* indicates the number of independent cultures. (**C**) Relative composition of *Tetraselmis* sp. cells grown under high and low nutrient conditions for 5 days. "Other" category refers to ash weight. Data depict mean ± SD of three independent cultures. (**D**) Absolute volume of cellular dry components and water in *Tetraselmis* sp. cells grown under high and low nutrient conditions for 5 days. Data depict mean ± SD of independent cultures ($N = 3$ to 4). (**E**) Same as (D), but the data are displayed as fractional water content (v/v). Dots depict independent cultures, and horizontal lines depict mean values. In (C) to (E), *P* values were obtained by unpaired *t* test.

nutrient specificity of sinking velocity regulation, we first tested which nutrient is responsible for starvation and increased cell sinking under our low nutrient conditions. We aimed to rescue starvation in the low nutrient *Tetraselmis* sp. cultures by different nutrient supplementations (Fig. 5A). While the addition of phosphorus, vitamins, or trace metals had no effect on cell growth on their own, the addition of nitrogen partially rescued cell growth, as measured by optical density (fig. S3C). Direct cell counts verified the rescue of cell growth by nitrogen supplementation, although phosphorus supplementation was also capable of a minor rescue in cell counts (Fig. 5B). Together, these results suggest that nitrogen is, at least initially, the growth-limiting nutrient under the low nutrient conditions used in this study, although phosphorus may also limit growth.

We then tested whether a rescue of the nitrogen limitation can reverse the increased sinking velocities observed under starvation. Supplementation with the complete high nutrient media rescued cell densities and sinking velocities near completely to the prestarvation levels (Fig. 5, C and D), indicating that the sinking velocity changes are reversible. Supplementation of starved cells with additional nitrogen also decreased cell densities and sinking velocities, although this rescue was not complete (Fig. 5, C and D). In contrast, supplementation with additional phosphorus increased cell densities and sinking velocities (Fig. 5, C and D). This is consistent with previous reports in *Tetraselmis subcordiformis*, where phosphorus increases carbohydrate storages under nitrogen limitation (*38*). Thus, our results indicate that nitrogen limitation is, at least partly, responsible for the increased sinking velocities in starved *Tetraselmis* sp.

Having established that nitrogen limitation can increase sinking velocities, we wanted to test whether the regulation of cell sinking velocities is similarly responsive to other nutrient limitations. We cultured *Tetraselmis* sp. under high nutrient conditions with a specific nutrient depleted for 5 days (Fig. 5E). All tested nutrient limitations (nitrogen, phosphorus, vitamins, or trace elements) increased cell densities and sinking velocities in comparison to the high nutrient conditions (Fig. 5, F and G). The sinking velocity increases were driven by cell mass and density increases rather than cell volume increases (fig. S3, A and B). We then correlated the cell proliferation rates across these conditions with the cell sinking velocities. This revealed a strong correlation (R^2 = 0.78; Fig. 5H), suggesting that the mechanism regulating cell sinking is coupled to the regulation of cell proliferation, when light is available.

Our results indicate that cell starvation, independently of the limiting nutrient, can increase sinking velocities. However, the regulation of size and composition is also affected by the nutrients that are not growth limiting, as indicated by the observation that phosphorus supplementation can increase sinking velocities further when nitrogen is growth limiting (Fig. 5, C and D). We therefore tested additional nutrient conditions by providing *Tetraselmis* sp. with a specific nutrient supplementation at the start of low nutrient culture (fig. S6A). As expected, the early nitrogen and phosphorus supplementation partially rescued cell proliferation (fig. S6B). However, nitrogen supplementation increased cell volumes by ~45% (fig. S6C), without altering cell densities (fig. S6D). In contrast, phosphorus supplementation had little effect on cell volumes but increased cell densities (fig. S6, C and D). Consequently, both nitrogen

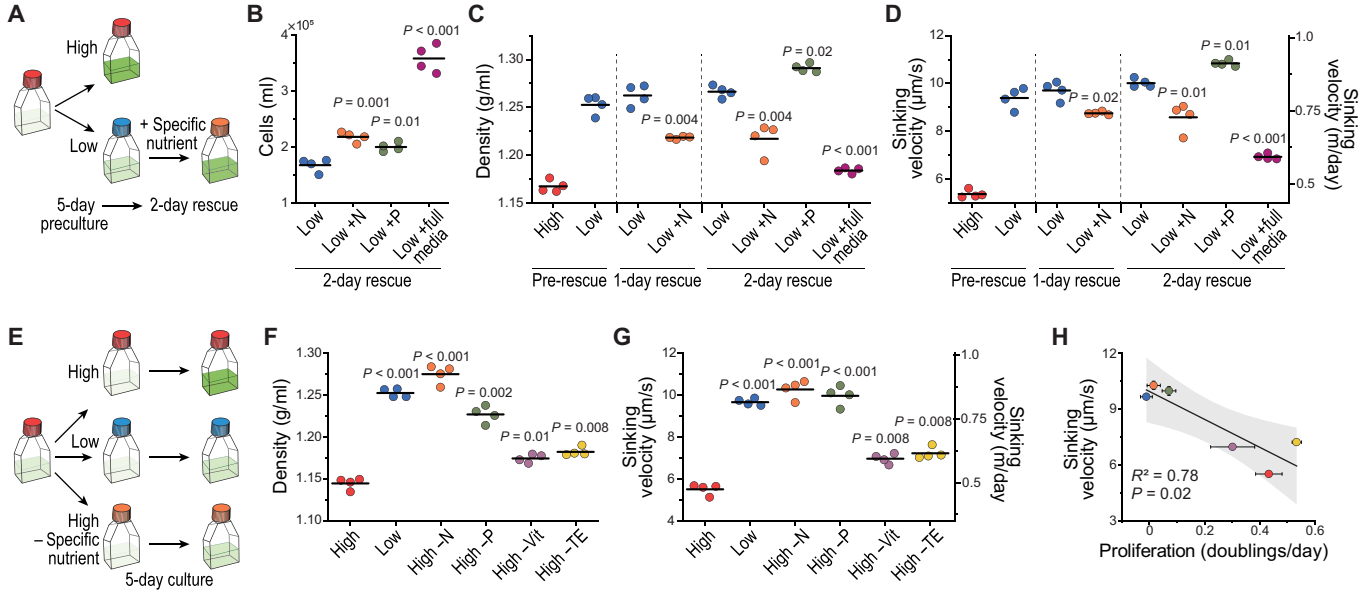

Fig. 5. *Tetraselmis* sp. sinking velocities respond to multiple nutrients and correlate with cell proliferation. (**A**) Experimental setup for identifying the limiting nutrient after 5-day culture under low nutrient conditions. (**B**) Cell counts 2 days after addition of indicated nutrient to the low nutrient culture. (**C** and **D**) *Tetraselmis* sp. cell densities (C) and sinking velocities (D) before and after addition of indicated nutrients to the low nutrient culture. *P* values were obtained by paired *t* test and depict comparisons to the low nutrient condition from the same day. (**E**) Experimental setup for testing nutrient limitations by specific nutrients. (**F** and **G**) *Tetraselmis* sp. cell densities (F) and sinking velocities (G) after 5-day culture under indicated nutrient condition. *P* values were obtained by paired *t* test and depict comparisons to the high nutrient condition. (**H**) Correlation between cell proliferation rate and sinking velocities in the samples used in (G). Dots and whiskers depict mean ± SEM. Black line and shaded area indicate a linear fit and 95% confidence band. In (B) to (G), N indicates nitrogen (orange), *P* indicates phosphorus (green), Vit indicates vitamins (light purple), and TE indicates trace elements (yellow). Dots depict independent cultures ($N = 4$), and horizontal lines depict mean values.

and phosphorus supplementation increased cell sinking velocities when supplied prestarvation (fig. S4E). Together, these results indicate that the mechanism regulating cell sinking integrates signals from multiple nutrients and that the availability of nitrogen and phosphorus can affect cell sinking differentially from each other.

DISCUSSION

We have introduced an approach for measuring gravitational sinking velocities across unicellular algae. Using our approach, we show that volume is a good predictor of gravitational sinking velocity (R^2 ~ 0.9) when examining vastly different sized species but less so when examining single cells within a species (R^2 ~ 0.5) or when comparing the same species under various environmental conditions. This is because cell volume can vary by orders of magnitude between species, while cell density cannot (densities outside the range of ~1.0 to 1.4 g/ml would require extraordinary compositional changes). We also revealed that algae follow the ⅔-power law scaling for cell volume–dependent sinking, both within and between species, although the degree of noise behind this scaling varies. This contrasts with a previous meta-analysis, which suggested that larger species sink significantly slower than expected based on the ⅔-power law scaling, possibly due to the extreme cell shapes examined (*33*). Notably, our results are specific to gravitational sinking, whereas previous analyses relied on data from cell settling experiments that are influenced by motility. In motile species, the ⅔-power law scaling of cell sinking may force larger cells to consume more energy to counteract excessive sinking. Because cell size increases in coordination with cell cycle progression (*39*–*41*), the size-dependent sinking within a species can also result in cell cycle–dependent vertical positioning of the cells in the ocean, as seen in some nonmotile species (*16*).

Cell compositional changes are known to affect cells' vertical movement in nonmotile algae (*14*–*18*). Our work has expanded this concept to motile algae, as we have revealed increased sinking velocities under starvation (stationary phase) due to increased cell densities in motile species. In *Tetraselmis* sp., we can mechanistically attribute the sinking velocity increases to a photosynthesis-driven accumulation of carbohydrates and a loss of intracellular water, both of which increase cell density (Fig. 4). This is consistent with observations in a related species, *T. subcordiformis*, where starvation increases starch production (*38*). Overall, our findings support the larger paradigm that uncoupling of photosynthesis and biosynthesis may have important biogeochemical consequences in part by influencing cell sinking (*42*, *43*).

On the basis of our observations, we propose a biological mechanism that contributes to the vertical movement of motile single cells in the marine carbon pump and nutrient cycles (Fig. 6). In the photic zone, photosynthesis drives the cellular accumulation of carbohydrates, which increases cell mass and density when nutrients (i.e., nitrogen) are not available to promote cell volume increases and proliferation. This, together with the loss of intracellular water, results in faster gravitational sinking, vertically transporting the cells to deeper ocean layers. This vertical movement may be supported by directed cell motility, especially because vertical transport that relies purely on gravitational sinking would take weeks (or even months) to transport cells from low to high nutrient zones in the ocean. However, gravitational sinking does not require energy, allowing cells to conserve their energy reservoirs for later upward movement.

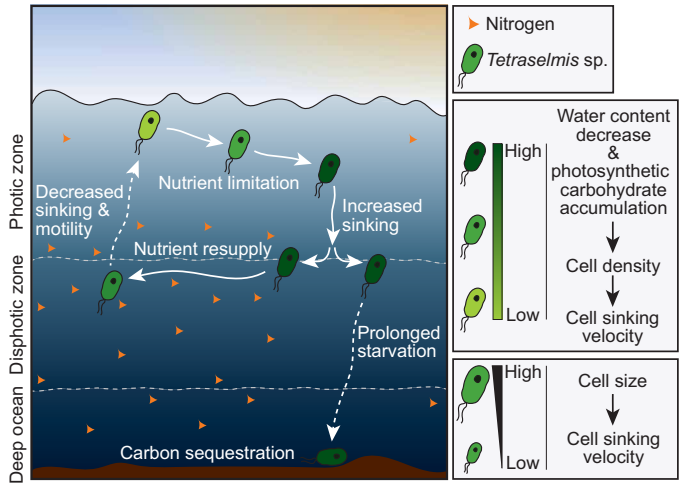

Fig. 6. Mechanistic basis for the ecology-dependent vertical movement of unicellular algae. Our results on *Tetraselmis* sp. suggest that the vertical movement of motile algae is partly reliant on the regulation of cell size and composition, which define the cell's gravitational sinking. In the photic zone, photosynthesis drives the accumulation of carbohydrates, which increases cell mass when other nutrients (i.e., nitrogen) are not available to promote cell volume increase and proliferation. Together with a loss of intracellular water, this results in higher cell density and faster gravitational sinking, transporting the cells to deeper ocean layers. If the cells encounter nutrients, then they can resume proliferation and decrease their gravitational sinking. The accumulated carbon storages may provide energy for upward motility. If the cells do not encounter nutrients as they sink, then prolonged starvation may result in cell death and eventual sequestration of the cell's carbon content at the ocean floor. In addition, the vertical cell positioning will also be affected by cell size, as sinking velocities scales with cell volumes according to the ⅔ power scaling.

If the cells encounter nutrients deeper, then they can resume proliferation and decrease their gravitational sinking to support vertical upward movement, as driven by motility and upwelling. *Tetraselmis* sp. can swim ~1 order of magnitude faster than the established gravitational sinking velocities (*44*), making upward migration from deeper ocean layers possible, given sufficient energy supply, which the accumulated carbohydrates may provide. Such ability of algae to vertically migrate long (~100 m) distances has been suggested before (*2*, *45*), especially for nonmotile species (*2*, *16*, *17*, *46*). We therefore propose that the regulation of gravitational sinking in motile algae could affect marine carbon and nutrient fluxes, and this should be further examined and possibly accounted for when modeling the marine nutrient and carbon fluxes (*10*, *11*).

Our work also provides further insights into the regulatory mechanism that controls cell sinking. We observed cases where sinking velocity increased due to cell density but not volume increases and other cases where sinking velocity increased due to cell volume but not density increases. Therefore, the regulation of cell sinking is at least partially independent of the regulation of cell size (volume regulation). This may be because cell volume can impose ecological constraints on the algae by influencing, for example, predation (grazing and viral infection), respiration, and light harvesting (*47*–*50*), whereas cell density is ecologically less constrained. The regulation of cell sinking can also integrate signals from multiple nutrients, as indicated by different cell sinking responses observed when supplementing the cells with nongrowth-limiting

nutrients. Further understanding of how these signals are integrated, and how they are coupled with cell proliferation, may enable external control of algae sinking that supports carbon capture and biomanufacturing (*51*).

Last, our work is a proof of methodology that could support research into marine ecology, algae cell biology, and the modeling of marine carbon and nutrient fluxes. As exemplified by our findings, our measurement approach is especially valuable in the study of motile unicellular algae whose motility prevents direct live cell investigations of gravitational sinking. While our measurements were carried out in artificial seawater medium and under laboratory conditions, our approach can be used to study a variety of algae in aquatic samples. With the development of automated sample preparation methods that separate large algae aggregates from single cells of different sizes, the SMR could be adapted for measurements of algae directly from the ocean. Such method development would enable high-throughput determination of sinking velocities in situ.

MATERIALS AND METHODS

Algal culture conditions

All algae were obtained from Provasoli-Guillard National Center for Marine Algae and Microbiota (NCMA) and belong to the Culture Collection of Marine Phytoplankton (CCMP), except for two coastal seawater isolates (A and B), which were both identified as *Thalassiosira* sp. according to 18*S* sequencing. Unialgal cultures were grown in filter-sterilized L1 or L1-Si medium, as appropriate for cell type (Table 1). Cultures were maintained at 20°C, and they received approximately 50 μm/s/m^2 of photosynthetically active radiation (PAR) as measured by a LI-COR LI-250 light meter. Cultures were transferred to fresh media weekly by a 1:10 dilution under a laminar flow hood and were regularly visually monitored for health (color, cell shape and size, purity, and motility when relevant) with microscopy.

For overall nutrient limitation experiments, two types of media were used: standard L1 or L1-Si for "high nutrient" conditions and L1/100 or L1-Si/100 for "low nutrient" conditions, in which the phosphorous, nitrate, trace metals, vitamins, and silica (if applicable) were diluted 1/100, while the salinity and pH of the medium remained unchanged. Algal cultures were pregrown in maintenance medium for 2 days under the light conditions detailed above. Cells were pelleted by centrifugation at 2600*g* for 10 min. The supernatant was discarded, and cells were washed once in artificial seawater (pH = 8.2) to prevent nutrient carryover. Cultures were then transferred to the appropriate medium for cell type and desired nutrient availability by a 1:10 dilution under a laminar flow hood and placed in the appropriate lighting condition for 5 days. The three lighting conditions used were "low light," in which light was available from nearby window at 50 μm/s/m^2 of PAR and day length varying between 9 and 15.3 hours depending on time of year (ambient temperature), "no light" in which cultures were incubated in a drawer without light exposure (ambient temperature), and "high light" in which cultures were grown with 100 μm/s/m^2 of PAR using full spectrum light-emitting diodes with a day-night cycle of 11 hours:13 hours in a temperature-controlled environmental chamber at 18°C. The typical daily variance in light availability under our low light conditions due to weather was ±5 μm/s per m^2 of PAR. All data in Fig. 1 are from species grown under low light and high nutrient conditions.

When defining the specific nutrient that limits cell growth and sinking velocity, cells were grown under low nutrient and low light conditions for 5 days, as detailed above, after which the culture medium was supplemented with indicated nutrients to rescue cell growth and/or sinking velocity. The nutrient concentrations used to

Table 1. List of species studied, their CCMP ID, and culture maintenance medium. N/A, not applicable.

Species	Class	Culture collection ID	Medium	Motility
M. pusilla	Mamelliophyceae	CCMP 1545	L1-Si	Motile
P. parkeae	Prasinophyceae	CCMP 725	L1-Si	Motile
Tetraselmis sp.	Chlorophyta	CCMP 908	L1-Si	Motile
Chlamydomonas sp.	Chlorophyta	CCMP 235	L1-Si	Motile
Rhodomonas salina	Cryptphyta	CCMP 1319	L1-Si	Motile
B. natans	Chloarachniophyta	CCMP 2755	L1-Si	Motile
N. oculata	Eustigmatophyta	CCMP 525	L1-Si	Nonmotile
Phaeodactylum tricornatum	Bacillariophyta	CCMP 632	L1	Nonmotile
Isolate A (*Thalassiosira* sp.)	Bacillariophyta	N/A	L1	Nonmotile
Isolate B (*Thalassiosira* sp.)	Bacillariophyta	N/A	L1	Nonmotile
Thalassiosira pseudonana	Bacillariophyta	CCMP 1335	L1	Nonmotile
P. minimum	Dinophyta	CCMP 1329	L1-Si	Motile
Phaeocystis globosa	Prymnesiophyceae	CCMP 629	L1-Si	Motile*
Emiliania huxleyi	Prymnesiophyceae	CCMP 2090	L1-Si	Nonmotile
E. huxleyi	Prymnesiophyceae	RCC 3962	L1-Si	Nonmotile
Isochrysis galbana	Prymnesiphyceae	CCMP 1323	L1-Si	Motile
Diachronema lutheri	Pavlovophyceae	CCMP 1325	L1-Si	Motile

*Motility is life cycle dependent, and designation reflects observations via light microscopy before measurements.

rescue cell growth and/or sinking velocity were identical to those found in the standard L1-Si media: 8.82 M $NaNO_3$, 3.62 M $NaH_2PO_4H_2O$, L1 vitamin solution, L1 trace element solution, and indicated combinations of these nutrients. The only exception to this was when rescuing cells with "full media" in Fig. 3, and the low nutrient media was diluted 1:1 with high nutrient media to avoid cell perturbations by centrifugation. The rescue efficiency was determined by cell counting and by optical density measurements at 600 nm 2 days following the nutrient spike-in.

Phylogeny construction and species verification

Purity and identity of all cultures were verified by Sanger sequencing of the V4-V9 region of the 18*S* rRNA gene. To amplify the 18*S* rRNA gene, cells were lysed by three consecutive freeze-thaw cycles, and 1 μl of lysate was added to the New England Biolabs Taq 5X MasterMix. The V4-V9 region was amplified using 570F (5′-CGG TAA YTC CAG CTC YAV) and EukB (5′-TGA TCC TTC TGC AGG TTC ACC TAC) primers added to a final concentration of 0.2 μM each. Polymerase chain reaction (PCR) cycling conditions were according to the manufacturer's specifications, with an annealing temperature of 52°C and extension time of 60 s. Purity of the amplification product was verified by gel electrophoresis, and PCR products were sequenced by Sanger sequencing at Azenta Life Sciences. The resulting sequences were searched by blastn against the National Center for Biotechnology Information (NCBI) nonredundant nucleotide collection to verify identity and purity of each strain.

The phylogeny was built by downloading the closest match full-length 18*S* sequence for each strain from NCBI, along with a representative of land plants, ameobae, and animals (NCBI accession numbers XR_004853735, AF114438, and M10098, respectively). Sequences were aligned using Mafft (*52*) v7.407 default parameters, alignments were trimmed using TrimAL (*53*) v1.2rev59 default parameters, and the tree was inferred using IQ-TREE (*54*) v1.6.8 with the model TIM2e + I + G4 as selected by the IQTree model finder. The resulting phylogeny was visualized and edited with FigTree (*55*) v1.4.4.

Microscopy-based volume and shape measurements

Cell volume and shape were determined by microscopy of unialgal cultures by EnviroScience Inc. (OH, USA). Live cultures were shipped overnight from Cambridge, MA to Stow, OH at ambient temperature. Upon arrival, 0.1 ml was placed into a Palmer-Maloney nano-plankton counting chamber and allowed to settle. In the case that cells are too motile to acquire clear images, the sample was fixed with 1 drop of Lugol's solution. A microscope-mounted camera was used to acquire images, and dimension and volume measurements were acquired by automated image processing software.

Macromolecular composition analysis

Tetraselmis sp. (CCMP 908) was pregrown in biological triplicates in maintenance medium for 2 days under our low light conditions and then transferred by a 1:10 dilution into 100 ml of L1-Si medium for the high nutrient condition and 250 ml of L1-Si/100 medium for the low nutrient condition. After 5 days of incubation under low light conditions, the cultures were pelleted by centrifuging at 10,000*g* for 15 min at 4°C, resulting in approximately 50 mg of wet biomass per replicate for both conditions. Samples were flash-frozen on a dry ice/ethanol bath and shipped on dry ice to the Bigelow Laboratory for Ocean Sciences (ME, USA), where subsequent analyses were performed by Bigelow Analytical Services. Briefly, dry mass was determined by lyophilizing samples and measuring on an analytical balance. Ash weight was determined as the proportion of initial dry weight remaining after the sample was placed in a muffle oven at 600°C for 16 hours. The proportion of protein in the dry mass was determined via the Dumas method using a Costech ECS 4010 elemental analyzer using a nitrogen-to-protein conversion factor of 4.76 (*56*). The proportion of lipid in the dry mass was determined by an amended gas chromatography–mass spectrometry method (*57*). Individual fatty acids were measured, and then all fatty acids were summed. The proportion of carbohydrates was determined indirectly as the remaining mass after accounting for water, ash, protein, and lipids.

Water content analysis

Tetraselmis sp. (CCMP 908) cells were prepared similarly to the molecular composition analysis described above, except using 10 ml of final volumes. After 5 days of culture in high and low nutrient media under low light conditions, cell total volumes were measured using Coulter counter, and the cell dry volumes were measured using an approach detailed previously (*23*, *36*). Briefly, the cell buoyant masses were measured with the SMR in normal water (H_2O) and in heavy water (D_2O)–based low nutrient media (same population measured separately in each condition). As heavy water exchanges with the water inside the cell, these two buoyant mass measurements can be used to calculate the average dry volume of the cells, when the solution densities are known. The solution densities were measured using the SMR, using NaCl solutions of known density for calibration. The calculated dry volumes were then compared to the Coulter counter–based total volume measurements to obtain the water content of the cells.

Cell count, buoyant mass, and volume measurements

Buoyant mass measurements were carried out using an SMR. The SMR is a vibrating cantilever with an internal microfluidic channel that allows single cells to travel through the interior of the cantilever. The resonant frequency of the cantilever changes due to the presence of a cell, and this change is proportional to buoyant mass of the cell. The fabrication and details of the operation of SMR are detailed in (*20*, *23*, *58*, *59*). This study used two different sizes of SMRs, one where the cantilever inner cross section is 8 μm by 8 μm and one where the cross section is 15 μm by 20 μm. Algae species with estimated diameter below 6 μm were measured using the smaller SMR, and larger algae species were measured using the larger SMR. For each measurement, an aliquot of cell culture was transferred to a vial fluidically connected to the SMR, and single cells were flushed through the SMR in culture media. Each cell measurement lasted <100 ms (travel time through the cantilever).

Cell volumes were measured using a Coulter counter (Multisizer 4, Beckman Coulter), which is based on the principle that a cell traversing an orifice filled with electrolyte will produce an impedance change proportional to the volume of the cell due to displacement of electrolyte. Algae cells were measured with one of two Coulter counter apertures, one 20 μm and one 100 μm in diameter, with the selection of aperture depending on cell size. Cell counting was also based on Coulter counter measurements. Each cell is measured in ~1 ms (travel time through the Coulter counter aperture). All measurements were carried out in culture media. The background noise

of the SMR and Coulter counter measurements were determined using a blank sample (no cells), and particles smaller than the reliable detection limit were not analyzed. When analyzing cell proliferation rates, cell counts were collected on days 4, 5, and 6 to calculate proliferation rate assuming exponential growth (the measurements that were used to derive sinking velocities were carried out on day 5).

When comparing different species, measurements were carried out between 10 a.m. and 6 p.m. This may result in minor biases in the measured cell sizes due to cell cycle synchronization with the light-dark cycle. All paired measurements of different nutrient conditions within the same species were carried out within 2 hours of each other to minimize biases due to cell cycle synchronization with the light-dark cycle. We note that some of the noise observed between our replicates for the species *Tetraselmis* sp. may be due to cell cycle synchronization (*60*) and different time of measurements for replicate experiments.

For SMR data analysis, the real-time resonant frequency data were analyzed by custom MATLAB code which detects the resonant frequency change caused by passage of a cell (*59*). The frequency change for each cell was converted to buoyant mass of the cell based on calibration using National Institute of Standards and Technology (NIST)–certified polystyrene beads (3 and 10 μm in diameter; Duke Standards, Thermo Fisher Scientific). For Coulter counter data analysis, cell volumes are automatically available from the instrument, and these values were recalibrated on the basis of measurements of NIST-certified polystyrene beads (2 and 6 μm in diameter; Duke Standards, Thermo Fisher Scientific).

Sinking velocity calculations

Algae sinking velocities were calculated according to the Stokes' law (Eq. 1), using the following values for environmental constants in surface ocean: the dynamic viscosity of seawater of 1.07×10^{-3} Pa·s at 20°C and the density of seawater of 1.02 g/ml. Both high and low nutrient culture media displayed similar densities, as quantified by SMR following a previously reported protocol (*21*, *61*). Cell radius was calculated from cell volume, and cell density was calculated using the volume and buoyant mass measurements (Eq. 2). In all algal species tested in this study, the Reynolds numbers did not exceed the scale of 10^{-7}.

The Stokes' law drag force was corrected to account for nonspherical cell shapes. The correction was carried out according to previous empirical results for a variety of shapes (*19*). The shape and aspect ratio for each species were first determined on the basis of microscopic images obtained in this study and/or provided by algae supplier (NCMA). A multiplicative shape factor was calculated for each species based on its shape and aspect ratio. All results shown in figures are without shape correction, as the calculated corrections were too minor to be clearly visible on the graphs (except for a single species, *P. tricornutum*).

Measurements to derive single-cell density and sinking velocity

Single-cell densities and sinking velocities were obtained by coupling buoyant mass measurements with fluorescence exclusion–based volume measurements (*24*) within the SMR device by building a fluorescence microscope on top of the SMR (*25*). In fluorescence exclusion measurements, the media contains a fluorophore, which is cell impermeable. When the fluorescence signal from a fixed volume is measured with and without a cell, the signal intensity decreases according to the volume of the cell as fluorescent media is excluded from the measurement volume. The volume measurement is independent of cell mass or density. In practice, cells were immersed in culture media containing fluorescein isothiocyanate–dextran (5 mg/ml; Sigma-Aldrich, catalog no. FD2000S; molecular weight, 2,000,000 g/mol) and flown through the SMR. Immediately after the SMR cantilever, the cells flowed through a fluorescence measurement area where the sample was exited with 482-nm light. Emission from the fluorescent dextran was collected with a photomultiplier tube using 515/30-nm emission filter. A typical measurement duration is 2 ms (time that the cell travels through the fluorescence measurement area).

SMR and fluorescence exclusion measurement data were paired using time information for each cell measurement, with a typical time lag between the two measurements being 10 ms. Cell volume was obtained by calculating the ratio between fluorescence signal decrease when a cell travels through the measurement area and the fluorescence baseline when a cell is not present in the measurement area. These cell volumes were then calibrated to absolute volume units by comparing the population size distributions to those measured with Coulter counter. Single-cell densities and sinking velocities were calculated from the buoyant mass and volume data as detailed above for population-level measurements.

Data analysis and statistics

In all figures, *n* refers to the number of single cells measured, while *N* refers to the number of independent experiments. Particles too small to be viable cells were removed from all final analyses. For analyses of single-cell density, particles with density above 1.7 g/ml were excluded, as these were likely due to mispairing of mass and volume measurements. For analyses of volume dependency, data were log-transformed and then fitted using a linear regression. When comparing volume dependency across species, reported errors for scaling exponent reflect the error of the fitted slope. When comparing volume dependency among single cells within a species, reported errors for scaling exponents reflect the error between independent experiments. Phylogenetically informed regression was performed by fitting a linear model to density, log-transformed volume or log-transformed sinking velocity and including the phylogeny as a covariate using the phylolm package (*62*) in R (2021). Pagel's lambda model was used for testing phylogeny as a covariate in our data. All other statistical details are indicated in the figures and figure legends, and details were calculated using OriginPro 2023 software.

Supplementary Materials

This PDF file includes:

Supplementary Note
Figs. S1 to S6
Legends for datasets S1 to S10
References

Other Supplementary Material for this manuscript includes the following:

Datasets S1 to S10

REFERENCES AND NOTES

1. C. B. Field, M. J. Behrenfeld, J. T. Randerson, P. Falkowski, Primary production of the biosphere: Integrating terrestrial and oceanic components. *Science* **281**, 237–240 (1998).

2. C. A. Durkin, B. A. S. Van Mooy, S. T. Dyhrman, K. O. Buesseler, Sinking phytoplankton associated with carbon flux in the Atlantic Ocean. *Limnol. Oceanogr.* **61**, 1172–1187 (2016).
3. A. Pantorno, D. P. Holland, S. Stojkovic, J. Beardall, Impacts of nitrogen limitation on the sinking rate of the coccolithophorid *Emiliania huxleyi* (Prymnesiophyceae). *Phycologia* **52**, 288–294 (2013).
4. E. Trudnowska, L. Lacour, M. Ardyna, A. Rogge, J. O. Irisson, A. M. Waite, M. Babin, L. Stemmann, Marine snow morphology illuminates the evolution of phytoplankton blooms and determines their subsequent vertical export. *Nat. Commun.* **12**, 2816 (2021).
5. D. M. Sigman, G. H. Haug, The biological pump in the past. *Treatise Geochem.* **6**, 491–528 (2003).
6. K. A. Miklasz, M. W. Denny, Diatom sinkings speeds: Improved predictions and insight from a modified Stokes' law. *Limnol. Oceanogr.* **55**, 2513–2525 (2010).
7. H. W. Ducklow, D. K. Steinberg, K. O. Buesseler, Upper ocean carbon export and the biological pump. *Oceanography* **14**, 50–58 (2001).
8. S. Dutkiewicz, M. J. Follows, J. G. Bragg, Modeling the coupling of ocean ecology and biogeochemistry. *Global Biogeochem. Cycles* **23**, 4017 (2009).
9. J. D. Wilson, O. Andrews, A. Katavouta, F. de Melo Viríssimo, R. M. Death, M. Adloff, C. A. Baker, B. Blackledge, F. W. Goldsworth, A. T. Kennedy-Asser, Q. Liu, K. R. Sieradzan, E. Vosper, R. Ying, The biological carbon pump in CMIP6 models: 21st century trends and uncertainties. *Proc. Natl. Acad. Sci. U.S.A.* **119**, e2204369119 (2022).
10. J. R. Palmer, I. J. Totterdell, Production and export in a global ocean ecosystem model. *Deep-Sea Res. I Oceanogr. Res. Pap.* **48**, 1169–1198 (2001).
11. J. S. Riley, R. Sanders, C. Marsay, F. A. C. Le Moigne, E. P. Achterberg, A. J. Poulton, The relative contribution of fast and slow sinking particles to ocean carbon export. *Global Biogeochem. Cycles* **26**, doi.org/10.1029/2011GB004085 (2012).
12. K. Wirtz, S. L. Smith, M. Mathis, J. Taucher, Vertically migrating phytoplankton fuel high oceanic primary production. *Nat Clim Chang* **12**, 750–756 (2022).
13. C. M. Moore, M. M. Mills, K. R. Arrigo, I. Berman-Frank, L. Bopp, P. W. Boyd, E. D. Galbraith, R. J. Geider, C. Guieu, S. L. Jaccard, T. D. Jickells, J. La Roche, T. M. Lenton, N. M. Mahowald, E. Marañón, I. Marinov, J. K. Moore, T. Nakatsuka, A. Oschlies, M. A. Saito, T. F. Thingstad, A. Tsuda, O. Ulloa, Processes and patterns of oceanic nutrient limitation. *Nat Geosci.* **6**, 701–710 (2013).
14. B. J. Gemmell, G. Oh, E. J. Buskey, T. A. Villareal, Dynamic sinking behaviour in marine phytoplankton: Rapid changes in buoyancy may aid in nutrient uptake. *Proc. R Soc. B Biol. Sci.* **283**, 20161126 (2016).
15. A. E. Walsby, D. P. Holland, Sinking velocities of phytoplankton measured on a stable density gradient by laser scanning. *J. R. Soc. Interface* **3**, 429–439 (2005).
16. A. G. Larson, R. Chajwa, H. Li, M. Prakash, Inflation induced motility for long-distance vertical migration. bioRxiv 504465 [Preprint] (2023). https://doi.org/10.1101/2022.08.19.504465.
17. V. S. Smetacek, Role of sinking in diatom life-history cycles: Ecological, evolutionary and geological significance. *Mar. Biol.* **84**, 239–251 (1985).
18. D. Titman, P. Kilham, Sinking in freshwater phytoplankton: Some ecological implications of cell nutrient status and physical mixing processes[1]. *Limnol. Oceanogr.* **21**, 409–417 (1976).
19. D. Leith, Drag on nonspherical objects. *Aerosol Sci. Tech.* **6**, 153–161 (2007).
20. T. P. Burg, M. Godin, S. M. Knudsen, W. Shen, G. Carlson, J. S. Foster, K. Babcock, S. R. Manalis, Weighing of biomolecules, single cells and single nanoparticles in fluid. *Nature* **446**, 1066–1069 (2007).
21. L. Mu, J. H. Kang, S. Olcum, K. R. Payer, N. L. Calistri, R. J. Kimmerling, S. R. Manalis, T. P. Miettinen, Mass measurements during lymphocytic leukemia cell polyploidization decouple cell cycle- And cell size-dependent growth. *Proc. Natl. Acad. Sci. U.S.A.* **117**, 15659–15665 (2020).
22. N. Cermak, J. W. Becker, S. M. Knudsen, S. W. Chisholm, S. R. Manalis, M. F. Polz, Direct single-cell biomass estimates for marine bacteria via Archimedes' principle. *ISME J.* **11**, 825–828 (2016).
23. T. P. Miettinen, K. S. Ly, A. Lam, S. R. Manalis, Single-cell monitoring of dry mass and dry mass density reveals exocytosis of cellular dry contents in mitosis. *eLife* **11**, e76664 (2022).
24. C. Cadart, E. Zlotek-Zlotkiewicz, L. Venkova, O. Thouvenin, V. Racine, M. Le Berre, S. Monnier, M. Piel, Fluorescence eXclusion Measurement of volume in live cells. *Methods Cell Biol.* **139**, 103–120 (2017).
25. W. Wu, S. H. Ishamuddin, T. W. Quinn, S. Yerrum, Y. Zhang, L. L. Debaize, P.-L. Kao, S. M. Duquette, M. A. Murakami, M. Mohseni, K.-H. Chow, T. P. Miettinen, K. L. Ligon, S. R. Manalis, Measuring single-cell density with high throughput enables dynamic profiling of immune cell and drug response from patient samples. bioRxiv 591092 [Preprint] (2024). https://doi.org/10.1101/2024.04.25.591092.
26. T. P. Miettinen, J. H. Kang, L. F. Yang, S. R. Manalis, Mammalian cell growth dynamics in mitosis. *eLife* **8**, e44700 (2019).
27. M. Alonso, F. C. Lago, J. M. Vieites, M. Espiñeira, Molecular characterization of microalgae used in aquaculture with biotechnology potential. *Aquaculture International* **20**, 847–857 (2012).
28. C. Lauritano, D. De Luca, M. Amoroso, S. Benfatto, S. Maestri, C. Racioppi, F. Esposito, A. Ianora, New molecular insights on the response of the green alga Tetraselmis suecica to nitrogen starvation. *Sci. Rep.* **9**, 3336 (2019).
29. C. A. Heil, P. M. Glibert, C. Fan, Prorocentrum minimum (Pavillard) Schiller. *Harmful Algae* **4**, 449–470 (2005).
30. G. E. Neurohr, A. Amon, Relevance and Regulation of Cell Density. *Trends Cell Biol.* **30**, 213–225 (2020).
31. E. Litchman, P. de Tezanos Pinto, K. F. Edwards, C. A. Klausmeier, C. T. Kremer, M. K. Thomas, Global biogeochemical impacts of phytoplankton: A trait-based perspective. *J. Ecol.* **103**, 1384–1396 (2015).
32. S. G. Leles, N. M. Levine, Mechanistic constraints on the trade-off between photosynthesis and respiration in response to warming. *Sci. Adv.* **9**, eadh8043 (2023).
33. G. Durante, A. Basset, E. Stanca, L. Roselli, Allometric scaling and morphological variation in sinking rate of phytoplankton. *J. Phycol.* **55**, 1386–1393 (2019).
34. A. Waite, A. Fisher, P. A. Thompson, P. J. Harrison, Sinking rate versus cell volume relationships illuminate sinking rate control mechanisms in marine diatoms. *Mar. Ecol. Prog. Ser.* **157**, 97–108 (1997).
35. D. R. Kellogg, P. A. Levin, Nutrient availability as an arbiter of cell size. *Trends Cell Biol.* **32**, 908–919 (2022).
36. F. Feijó Delgado, N. Cermak, V. C. Hecht, S. Son, Y. Li, S. M. Knudsen, S. Olcum, J. M. Higgins, J. Chen, W. H. Grover, S. R. Manalis, Correction: Intracellular water exchange for measuring the dry mass, water mass and changes in chemical composition of living cells. *PLOS ONE* **8**, e67590 (2013).
37. H. Shi, C. S. Westfall, J. Kao, P. D. Odermatt, S. E. Anderson, S. Cesar, M. Sievert, J. Moore, C. G. Gonzalez, L. Zhang, J. E. Elias, F. Chang, K. C. Huang, P. A. Levin, Starvation induces shrinkage of the bacterial cytoplasm. *Proc. Natl. Acad. Sci. U.S.A.* **118**, e2104686118 (2021).
38. C. Yao, J. Jiang, X. Cao, Y. Liu, S. Xue, Y. Zhang, Phosphorus enhances photosynthetic storage starch production in a green microalga (Chlorophyta) *Tetraselmis subcordiformis* in nitrogen starvation conditions. *J. Agric. Food Chem.* **66**, 10777–10787 (2018).
39. T. P. Miettinen, M. J. Caldez, P. Kaldis, M. Björklund, Cell size control–a mechanism for maintaining fitness and function. *Bioessays* **39**, (2017).
40. A. A. Amodeo, J. M. Skotheim, Cell-size control. *Cold Spring Harb. Perspect. Biol.* **8**, a019083 (2016).
41. C. Cadart, L. Venkova, P. Recho, M. C. Lagomarsino, M. Piel, The physics of cell-size regulation across timescales. *Nat. Phys.* **15**, 993–1004 (2019).
42. K. H. Halsey, B. M. Jones, Phytoplankton strategies for photosynthetic energy allocation. *Ann. Rev. Mar. Sci.* **7**, 265–297 (2015).
43. Z. Wu, S. Dutkiewicz, O. Jahn, D. Sher, A. White, M. J. Follows, Modeling photosynthesis and exudation in subtropical oceans. *Global Biogeochem. Cycles* **35**, e2021GB006941 (2021).
44. S. R. Erga, M. Dybwad, Ø. Frette, J. K. Lotsberg, K. Aursland, New aspects of migratory behavior of phytoplankton in stratified waters: Effects of halocline strength and light on Tetraselmissp. (Prasinophyceae) in an artificial water column. *Limnol. Oceanogr.* **48**, 1202–1213 (2003).
45. K. Wirtz, S. L. Smith, Vertical migration by bulk phytoplankton sustains biodiversity and nutrient input to the surface ocean. *Sci. Rep.* **10**, 1142 (2020).
46. T. A. Villareal, C. Pilskaln, M. Brzezinski, F. Lipschultz, M. Dennett, G. B. Gardner, Upward transport of oceanic nitrate by migrating diatom mats. *Nature* **397**, 423–425 (1999).
47. B. C. Monger, M. R. Landry, Prey-size dependency of grazing by free-living marine flagellates*. *Mar. Ecol. Prog. Ser.* **74**, 239–248 (1991).
48. A. G. Murray, G. A. Jackson, Viral dynamics: A model of the effects of size shape, motion and abundance of single-celled olanktonic organisms and other particles. *Mar. Ecol. Prog. Ser.* **89**, 103–116 (1992).
49. H. Hillebrand, E. Acevedo-Trejos, S. D. Moorthi, A. Ryabov, M. Striebel, P. K. Thomas, M. L. Schneider, Cell size as driver and sentinel of phytoplankton community structure and functioning. *Funct Ecol* **36**, 276–293 (2022).
50. K. H. Andersen, A. W. Visser, From cell size and first principles to structure and function of unicellular plankton communities. *Prog. Oceanogr.* **213**, 102995 (2023).
51. M. G. Schubert, T.-C. Tang, I. M. Goodchild-Michelman, K. A. Ryon, J. R. Henriksen, T. Chavkin, Y. Wu, T. P. Miettinen, S. Van Wychen, L. R. Dahlin, D. Spatafora, G. Turco, M. T. Guarnieri, S. R. Manalis, J. Kowitz, R. Dhir, P. Quatrini, C. E. Mason, G. M. Church, M. Milazzo, B. T. Tierney, Cyanobacteria newly isolated from marine volcanic seeps display rapid sinking and robust, high density growth. bioRxiv 564770 [Preprint] (2023). https://doi.org/10.1101/2023.10.30.564770.
52. K. Katoh, D. M. Standley, MAFFT multiple sequence alignment software version 7: Improvements in performance and usability. *Mol. Biol. Evol.* **30**, 772–780 (2013).
53. S. Capella-Gutiérrez, J. M. Silla-Martínez, T. Gabaldón, trimAl: A tool for automated alignment trimming in large-scale phylogenetic analyses. *Bioinformatics* **25**, 1972–1973 (2009).
54. L. T. Nguyen, H. A. Schmidt, A. Von Haeseler, B. Q. Minh, IQ-TREE: A fast and effective stochastic algorithm for estimating maximum-likelihood phylogenies. *Mol. Biol. Evol.* **32**, 268–274 (2015).

55. A. Rambaut, FigTree–v. 1.4.4, a graphical viewer of phylogenetic trees; http://tree.bio.ed.ac.uk/software/figtree/ (2018).
56. A. Schwenzfeier, P. A. Wierenga, H. Gruppen, Isolation and characterization of soluble protein from the green microalgae *Tetraselmis* sp. *Bioresour. Technol.* **102**, 9121–9127 (2011).
57. G. Breuer, W. A. C. Evers, J. H. de Vree, D. M. M. Kleinegris, D. E. Martens, R. H. Wijffels, P. P. Lamers, Analysis of fatty acid content and composition in microalgae. *J. Vis. Exp.*, 10.3791/50628 (2013).
58. S. Olcum, N. Cermak, S. C. Wasserman, K. S. Christine, H. Atsumi, K. R. Payer, W. Shen, J. Lee, A. M. Belcher, S. N. Bhatia, S. R. Manalis, Weighing nanoparticles in solution at the attogram scale. *Proc. Natl. Acad. Sci. U.S.A.* **111**, 1310–1315 (2014).
59. J. H. Kang, T. P. Miettinen, L. Chen, S. Olcum, G. Katsikis, P. S. Doyle, S. R. Manalis, Noninvasive monitoring of single-cell mechanics by acoustic scattering. *Nat. Methods* **16**, 263–269 (2019).
60. J. Fábregas, M. Patiño, E. Vecino, F. Cházaro, A. Otero, Productivity and biochemical composition of cyclostat cultures of the marine microalga Tetraselmis suecica. *Appl. Microbiol. Biotechnol.* **43**, 617–621 (1995).
61. W. H. Grover, A. K. Bryan, M. Diez-Silva, S. Suresh, J. M. Higgins, S. R. Manalis, Measuring single-cell density. *Proc. Natl. Acad. Sci. U.S.A.* **108**, 10992–10996 (2011).
62. L. S. Tung Ho, C. Ané, A linear-time algorithm for gaussian and non-gaussian trait evolution models. *Syst. Biol.* **63**, 397–408 (2014).
63. C. M. Boyd, D. Gradmann, Impact of osmolytes on buoyancy of marine phytoplankton. *Mar. Biol.* **141**, 605–618 (2002).
64. T. H. Gouw, J. C. Vlugter, Physical Properties of Triglycerides. I. Density and Refractive Index. *Fette, Seifen, Anstrichmittel* **68**, 544–549 (1966).
65. R. Milo, P. Jorgensen, U. Moran, G. Weber, M. Springer, BioNumbers—the database of key numbers in molecular and cell biology. *Nucleic Acids Res.* **38**, D750–D753 (2010).
66. H. Pereira, J. Silva, T. Santos, K. N. Gangadhar, A. Raposo, C. Nunes, M. A. Coimbra, L. Gouveia, L. Barreira, J. Varela, Nutritional potential and toxicological evaluation of tetraselmis sp. CTP4 microalgal biomass produced in industrial photobioreactors. *Molecules* **24**, 3192 (2019).
67. S. Paterson, P. Gómez-Cortés, M. A. de la Fuente, B. Hernández-Ledesma, Bioactivity and digestibility of microalgae *Tetraselmis* sp. and *Nannochloropsis* sp. as basis of their potential as novel functional foods. *Nutrients* **15**, 477 (2023).
68. J. Valenzuela, A. Mazurie, R. P. Carlson, R. Gerlach, K. E. Cooksey, B. M. Peyton, M. W. Fields, Potential role of multiple carbon fixation pathways during lipid accumulation in *Phaeodactylum tricornutum*. *Biotechnol. Biofuels* **5**, 1–17 (2012).

Acknowledgments

Funding: This work was supported by the Simons Foundation (Life Sciences Project Award–572792) to M.F.P. and S.R.M. and the National Science Foundation (Award 2319028) to S.R.M. **Author contributions:** T.P.M., A.L.G., Y.W., M.F.P., and S.R.M. conceived and designed the research; T.P.M., A.L.G., Y.W., W.W., T.R.U., and Y.H. carried out the experiments; T.P.M., A.L.G., Y.W., and B.R.K.R. analyzed the data; B.R.K.R., M.F.P., and S.R.M. provided resources and conceptual feedback; and T.P.M., A.L.G., and Y.W. wrote the paper with input from all authors. **Competing interests:** S.R.M. is a cofounder of and affiliated with the companies Travera and Affinity Biosensors, which develop techniques relevant to the research presented. S.R.M., W.W., and T.P.M. are inventors on patent application (PCT/US2022/051503) submitted by MIT that covers single-cell density measurement technology. All other authors declare that they have no competing interests. **Data and materials availability:** All data needed to evaluate the conclusions in the paper are present in the paper and/or the Supplementary Materials. All buoyant mass and volume data, which were used to calculate cell densities and sinking velocities, are included in the datasets S1 to S10. For details about the supplementary datasets, please see the first datasheet (readme) in the supplementary data file.

Submitted 2 January 2024
Accepted 4 June 2024
Published 5 July 2024
10.1126/sciadv.adn8356